

# Journal of Materials Chemistry B

Accepted Manuscript



This is an *Accepted Manuscript*, which has been through the Royal Society of Chemistry peer review process and has been accepted for publication.

*Accepted Manuscripts* are published online shortly after acceptance, before technical editing, formatting and proof reading. Using this free service, authors can make their results available to the community, in citable form, before we publish the edited article. We will replace this *Accepted Manuscript* with the edited and formatted *Advance Article* as soon as it is available.

You can find more information about *Accepted Manuscripts* in the [Information for Authors](#).

Please note that technical editing may introduce minor changes to the text and/or graphics, which may alter content. The journal's standard [Terms & Conditions](#) and the [Ethical guidelines](#) still apply. In no event shall the Royal Society of Chemistry be held responsible for any errors or omissions in this *Accepted Manuscript* or any consequences arising from the use of any information it contains.

# A series of triphenylamine-based two-photon absorbing materials with AIE property for biological imaging

Yanqiu Liu,<sup>a</sup> Ming Kong,<sup>a</sup> Qiong Zhang,<sup>a</sup> Zhiwen Zhang,<sup>a</sup> Hongping Zhou,<sup>a</sup> Shengyi Zhang,<sup>a</sup> Shengli Li,<sup>a</sup> Jieying Wu,<sup>\*a</sup> Yupeng Tian<sup>\*a</sup>

<sup>5</sup> Received (in XXX, XXX) Xth XXXXXXXXX 200X, Accepted Xth XXXXXXXXX 200X

First published on the web Xth XXXXXXXXX 200X

DOI: 10.1039/b000000x

A specific series of D- $\pi$ -A (**1A-3A**) and D- $\pi$ -D (**1B-3B**) structural chromophores with various electron donors and  $\pi$ -conjugated bridges were designed, synthesized, and fully characterized. Their crystal structures were determined by single crystal X-ray diffraction analysis. The one/two-photon absorption properties of the chromophores have been successfully tuned by using different electron donors and  $\pi$ -bridges. Interestingly, it was found that chromophore **3B** shows quite weakly fluorescent in pure DMSO, while a significant AIE (aggregation-induced emission) effect is observed in water/DMSO (v/v 90%) mixtures with a sharp increase in fluorescence intensity about 11 times. Furthermore, chromophore **3B** shows strong two-photon excited fluorescence (TPEF) and large 2PA action cross section (394 GM). The results of live-cell imaging experiments show that **3B** can be effectively used as a bio-imaging probe in two-photon fluorescence microscopy towards HepG2 cells *in vitro*. The TPEF images of **3B** not only exhibit cellular cytosol uptake but also exhibit actin regulatory protein uptake which are different from OPEF images.

## 20 Introduction

Organic molecules with large two-photon absorption (2PA) draw great interest in the field of material science due to their various applications including optical limiting,<sup>1-3</sup> up-converted lasing,<sup>4</sup> 3D optical data storage,<sup>5</sup> micro-fabrication,<sup>6</sup> bio-imaging,<sup>7</sup> and photodynamic therapy.<sup>8</sup> With the significant potential applications, a large amount of compounds with large 2PA cross sections ( $\sigma$ ) and good processabilities have been developed. The molecular design strategies include symmetrical donor-acceptor-donor (D-A-D), donor- $\pi$ -bridge-acceptor (D- $\pi$ -A), and donor- $\pi$ -bridge-donor (D- $\pi$ -D) structure.<sup>9-16</sup> These studies revealed that the intramolecular charge transfer (ICT) from the donor groups to the  $\pi$ -bridge can enhance the 2PA cross sections. Other factors such as strength of the donor and acceptor, the character of the conjugated bridge, the planarity of the chromophores, and the dimensionality of the charge-transfer network<sup>17</sup> can also enhance the 2PA cross section.

For bio-photonics applications, a good 2PA labeling agent with a high 2PA cross section and large 2PA action cross section ( $\Phi\sigma$ , where  $\Phi$  is the fluorescence quantum yield) is highly desired. It is necessary that 2PA chromophores are water soluble or dispersible and remain highly fluorescent in aqueous media. However, highly efficient 2PA fluorescence has suffered the defect of low fluorescence efficiency in aqueous media because most 2PA molecules are hydrophobic and their fluorescence quantum yields are considerably reduced in water, by self-aggregation, which generally leads to fluorescence quenching.<sup>18</sup> To overcome this limitation, a special molecular design for a 2PA chromophore is required

not only to ensure a large two-photon activity, but more importantly, to overcome fluorescence quenching at high concentration or in biological aqueous environment, which is generally observed for common organic fluorophores. Recently, some novel 2PA chromophores were synthesized both with large two-photon activity and high fluorescence quantum yields in aggregation. Prasad and co-workers had synthesized a chromophore with aggregation-enhanced fluorescence and two-photon absorption in nano-aggregates due to the hindering of molecular internal rotation.<sup>19</sup> Tang discovered luminogenic molecules and polymers of AIE and 2PA based on tetraphenylethene.<sup>20</sup> Recently, our group have reported several series of compounds based on isophorone<sup>21</sup> or triphenylamine<sup>22</sup> with good AIE property.

Triphenylamine has been widely used in opto- and electro-active materials for the good electron-donating and transporting capabilities, as well as their special propeller starburst molecular structure.<sup>23, 24</sup> Recently, 2PA materials with triphenylamine as the electron donor have aroused great interest and become the focus of intensive research in this field.<sup>25, 26</sup> Ethoxyl was also attached to the triphenylamine group to enhance its electron-donating ability and improve solubility of the compounds. Moreover, cyano-substituted compounds show good optical and electrical properties due to their high electron affinities. Molecules including an electron-withdrawing cyano group on the central  $\pi$ -bridge exhibit strong fluorescence and higher 2PA cross section value.<sup>27, 28</sup> Some cyano-substituted compounds have been reported to show unique enhanced emission rather than a fluorescence quenching in the solid state,<sup>29, 30</sup> which enlightened us to design the novel functional molecules with both AIE and 2PA properties. In this present, we report

synthesis and optical properties (linear and nonlinear) of the six novel type D- $\pi$ -A (**1A-3A**) and D- $\pi$ -D (**1B-3B**) chromophores (Scheme 1) based on cyano-substituted triphenylamine with derivatives. The correlation between molecular structures and spectral properties are discussed by quantum-chemical calculation and X-ray crystallography. Interestingly, a simple modification on  $\pi$ -bridge of chromophore **3B** results in good AIE characteristic together with fascinating 2PA properties compared with other related chromophores, suggesting the suitability of **3B** for high-contrast bio-imaging application.

## Experimental Section

### General procedures

All chemicals were commercially available and use as obtained. The solvents were purified by conventional methods before used. IR spectra were recorded with a Nicolet FT-IR NEXUS 870 spectrometer (KBr discs) in the 4000-400  $\text{cm}^{-1}$  region.  $^1\text{H}$  and  $^{13}\text{C}$  NMR spectra were recorded on a 400 and 100 MHz NMR instrument using  $(\text{CD}_3)_2\text{SO}$  or  $(\text{CD}_3)_2\text{CO}$  as solvent. Chemical shifts were reported in parts per million (ppm) relative to internal TMS (0 ppm) and coupling constants in Hz. Splitting patterns were described as singlet (s), doublet (d), triplet (t), quartet (q), or multiplet (m). MALDI-TOF mass spectra were recorded on a time-of-flight (TOF) mass spectrometer using a 337 nm nitrogen laser with alpha-cyano-4-hydroxycinnamic acid as matrix.

### Optical measurements

The one-photon absorption (OPA) spectra were obtained on a UV-265 spectrophotometer. The one-photon excited fluorescence (OPEF) spectra measurements were performed using a Hitachi F-7000 fluorescence spectrophotometer. OPA and OPEF of all chromophores were measured in five organic solvents of different polarities with the concentration of  $1.0 \times 10^{-5} \text{ mol}\cdot\text{L}^{-1}$ . The quartz cuvettes used are of 1 cm path length. The fluorescence quantum yields ( $\Phi$ ) were determined by using coumarin 307 as the reference according to the literature method.<sup>31</sup> Quantum yields were corrected as follows:

$$\Phi_s = \Phi_r \left( \frac{A_r \eta_s^2 D_s}{A_s \eta_r^2 D_r} \right)$$

Where the  $s$  and  $r$  indices designate the sample and reference samples, respectively,  $A$  is the absorbance at  $\lambda_{exc}$ ,  $\eta$  is the average refractive index of the appropriate solution, and  $D$  is the integrated area under the corrected emission spectrum.<sup>32</sup>

For time-resolved fluorescence measurements, the fluorescence signals were collimated and focused onto the entrance slit of a monochromator with the output plane equipped with a photomultiplier tube (HORIBA HuoroMax-4P). The decays were analyzed by 'least-squares'. The quality of the exponential fits was evaluated by the goodness of fit ( $\chi^2$ ).

Two-photon absorption (2PA) cross sections ( $\sigma$ ) of the samples were obtained by two-photon excited fluorescence (TPEF)

method<sup>33</sup> at femtosecond laser pulse and Ti: sapphire system (680-1080 nm, 80 MHz, 140 fs, Chameleon II) as the light source. The sample was dissolved in benzene solvent at a concentration of  $1.0 \times 10^{-3} \text{ mol}\cdot\text{L}^{-1}$ . The intensities of TPEF spectra of the reference and the sample were determined at their excitation wavelength. Thus,  $\sigma$  of samples was determined by the following Eq.,

$$\sigma = \sigma_{ref} \frac{F \cdot \Phi_{ref} \cdot C_{ref} \cdot n_{ref}}{F_{ref} \cdot \Phi \cdot C \cdot n}$$

Where the  $ref$  subscripts stand for the reference molecule (here fluorescein in the aqueous NaOH solution ( $1 \text{ mol}\cdot\text{L}^{-1}$ ) at concentration of  $1.0 \times 10^{-3} \text{ mol}\cdot\text{L}^{-1}$  was used as reference).  $\sigma$  is the 2PA cross-section value,  $c$  is the concentration of the solution,  $n$  is the refractive index of the solution,  $F$  is the TPEF integral intensities of the solution emitted at the exciting wavelength, and  $\Phi$  is the fluorescence quantum yield. The  $\sigma_{ref}$  value of reference was taken from the literature.<sup>34</sup>

### Computational studies

Density functional theory (DFT) calculations on all the compounds were carried out in vacuo for a better understanding of the charge transfer state. Optimizations were carried out with B3LYP[LANL2DZ] without any symmetry restraint, and the time-dependent density functional theory (TD-DFT) {B3LYP[LANL2DZ]} calculations were performed on the optimized structure.<sup>35</sup> All calculations, including optimizations and TD-DFT, were performed with the G03 software.<sup>36</sup> Geometry optimization of the singlet ground state and the TD-DFT calculation of the lowest 25 singlet-singlet excitation energies were calculated with a basis set composed of 6-31 G\* for C H N O atoms were downloaded from the EMSL basis set library.

### X-ray structural determinations

Single crystals of the compounds used in X-ray determination were obtained by slow evaporation of their mother liquors. X-ray diffraction data of **1A-3A** and **3B** were collected on a Bruker Smart 100 CCD area detector diffractometer. Both of the radiation sources were Mo  $K\alpha$  ( $\lambda = 0.71073 \text{ \AA}$ ). Empirical absorption correction was applied to the data. The structures were solved by direct methods and refined by full-matrix least-squares methods on  $F^2$ . All the nonhydrogen atoms were located from the trial structure and then refined anisotropically with SHELXTL using the full matrix least-squares procedure.<sup>37</sup> The hydrogen atom positions were geometrically idealized and generated in idealized positions and fixed displacement parameters. Cambridge Crystallographic Data Centre (CCDC) as supplementary publication numbers CCDC **1A-854148** (see ref. 39), **2A-1006493**, **3A-1006514**, **3B-1006515**.

### Cell image

HepG2 cells were seeded in 6 well plates at a density of  $2 \times 10^5$  cells per well and grown for 96 h. For live cell imaging cell cultures were incubated with the complexes (10% PBS: 90% cell media) at concentration of 40  $\mu\text{M}$  and maintained at 37  $^\circ\text{C}$  in an atmosphere of 5%  $\text{CO}_2$  and 95% air for incubation times ranging

for 2 h. The cells were then washed with PBS (3 × 3 mL per well) and 3 mL of PBS was added to each well. The cells were imaged using confocal laser scanning microscopy and water immersion lenses. Excitation energy of 720 nm was used and the fluorescence emission was measured at 495-582 nm.

HepG2 cells were luminescently imaged on a Zeiss LSM 710 META upright confocal laser scanning microscope using magnification 40 × and 100 × water-dipping lenses for monolayer cultures. Image data acquisition and processing was performed using Zeiss LSM Image Browser, Zeiss LSM Image Expert and Image J.

### Cytotoxicity assays in cells

To ascertain the cytotoxic effect of all the compounds treatment over a 24 h period, the 5-dimethylthiazol-2-yl-2,5-diphenyl-tetrazolium bromide (MTT) assay was performed. HepG2 cells were trypsinized and plated to ~70% confluence in 96-well plates 24 h before treatment. Prior to the treatment of compounds, the DMEM was removed and replaced with fresh DMEM, and aliquots of the compound stock solutions (500 μM DMSO) were added to obtain final concentrations of 0, 10, 20, 40, 60, and 80 μM. The treated cells were incubated for 24 h at 37 °C and under 5% CO<sub>2</sub>. Subsequently, the cells were treated with 5 mg/mL MTT (40 μL/well) and incubated for an additional 4 h (37 °C, 5% CO<sub>2</sub>). Then, DMEM was removed, the formazan crystals were dissolved in DMSO (150 μL/well), and the absorbance at 490 nm was recorded. The cell viability (%) was calculated according to the following equation: cell viability % = OD<sub>490</sub>(sample)/OD<sub>490</sub>(control) × 100, where OD<sub>490</sub>(sample) represents the optical density of the wells treated with various concentration of the compounds and OD<sub>490</sub>(control) represents that of the wells treated with DMEM + 10% FCS. Three independent trials were conducted, and the averages and standard deviations are reported. The reported percent cell survival values are relative to untreated control cells.

### Synthesis

The chromophores **1A** and **1B** were prepared as literature.<sup>38</sup>

**N-(4-(4-nitrostyryl)phenyl)-4-ethoxy-N-(4ethoxyphenyl)benzenamine (2A)**. diethyl(4-nitrophenyl)methylphosphonate (**M1**) (2.73 g, 10 mmol), t-BuOK (2.24 g, 20 mmol), 4-(bis(4-ethoxyphenyl)amino)benzaldehyde (**M2**) (3.61 g, 10 mmol), and a modicum of 18-crown-6 were placed into a dry mortar. The mixture milled vigorously for about 20 min, after completion of the reaction (monitored by TLC), the mixture was dissolved in 150 mL CH<sub>2</sub>Cl<sub>2</sub> and washed with Di-water, the organic layer was separated and dried over MgSO<sub>4</sub>, filtered and solvent was removed in vacuo. The product was purified by recrystallization from anhydrous ethanol to get 2.41 g dark red crystals. Yield: 51%. IR (KBr, cm<sup>-1</sup>): 2978, 2924, 1580, 1504, 1476, 1391, 1334, 1239, 954, 834. <sup>1</sup>H-NMR (400 MHz, (CD<sub>3</sub>)<sub>2</sub>SO) δ (ppm): 8.20 (d, *J* = 8.80 Hz, 2H), 7.79 (d, *J* = 8.80 Hz, 2H), 7.46 (m, 3H), 7.19 (d, *J* = 16.0 Hz, 1H), 7.08 (d, *J* = 8.80 Hz, 4H), 6.92 (d, *J* = 8.80 Hz, 4H), 6.83 (d, *J* = 8.80 Hz, 2H), 4.04 (q, *J* = 6.80 Hz, 4H), 1.37 (t, *J* = 6.80 Hz, 6H). <sup>13</sup>C-NMR (100 MHz, (CD<sub>3</sub>)<sub>2</sub>SO) δ (ppm): 156.98, 150.51, 145.90, 140.86, 134.17, 128.14, 127.46,

123.97, 119.79, 116.27, 64.24, 15.16. MALDI-TOF Calcd for C<sub>30</sub>H<sub>28</sub>N<sub>2</sub>O<sub>4</sub>, 480.21; Found, 480.25.

**N-(4-(4-aminostyryl)phenyl)-4-ethoxy-N-(4-ethoxyphenyl)benzenamine (2B)**. **2A** (0.96 g, 2 mmol) was dissolved in ethanol (25 mL) and added into a round-bottom flask equipped with a magnetic stirrer then heated to 80 °C. 0.06 g Pd/C catalyst was added into the preceding reaction system and a solution of ethanol (25 mL) contained 85% hydrazine hydrate (5 mL) was added dropwise for 0.5 h. After the reaction completed, the solvent was removed under reduced pressure. The mixture was washed with water and extracted with ethyl acetate. The organic phase was dried over MgSO<sub>4</sub>, filtered and concentrated to provide light red oil. Purified by silica gel column chromatography using petroleum ether (b.p. 60-90 °C)/ethyl acetate (10:1 by volume) to get 0.55 g yellow powder. Yield: 60%. IR (KBr, cm<sup>-1</sup>): 3452, 3374, 3028, 2979, 2925, 1607, 1503, 1476, 1392, 1283, 1238, 1046, 962, 827. <sup>1</sup>H-NMR (400 MHz, (CD<sub>3</sub>)<sub>2</sub>SO), δ (ppm): 7.31 (d, *J* = 8.8 Hz, 2H), 7.21 (d, *J* = 8.4 Hz, 2H), 6.97 (d, *J* = 8.8 Hz, 4H), 6.88 (t, 5H), 6.82 (d, *J* = 13.2 Hz, 1H), 6.73 (d, *J* = 8.8 Hz, 2H), 6.54 (d, *J* = 8.4 Hz, 2H), 5.22 (s, 2H), 3.99 (q, *J* = 6.9 Hz, 4H), 1.32 (t, *J* = 6.8 Hz, 6H). <sup>13</sup>C-NMR (100 MHz, (CD<sub>3</sub>)<sub>2</sub>SO) δ (ppm): 154.83, 148.24, 146.92, 140.03, 130.21, 127.16, 126.52, 126.30, 125.16, 122.56, 119.84, 115.34, 113.90, 63.13, 14.68. MALDI-TOF Calcd for C<sub>30</sub>H<sub>30</sub>N<sub>2</sub>O<sub>2</sub>, 450.23; Found, 450.28.

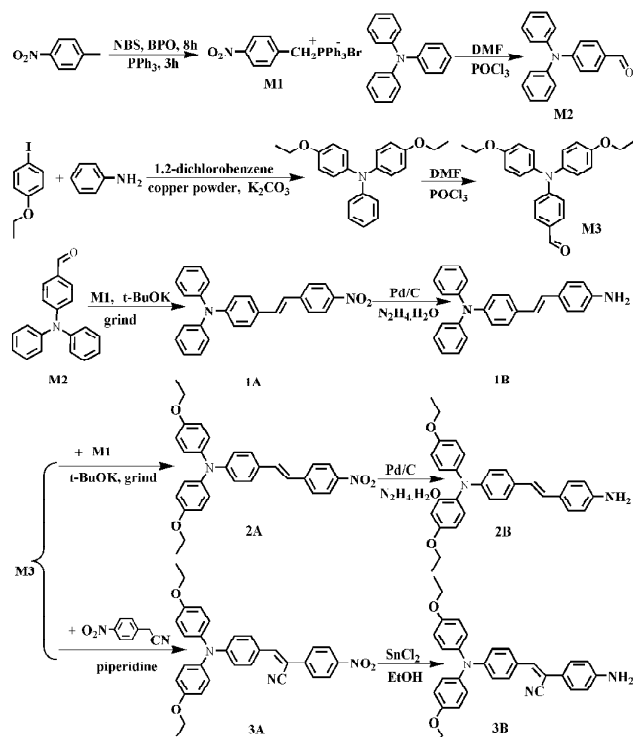
**(Z)-3-(4-(bis(4-ethoxyphenyl)amino)phenyl)-2-(4-nitrophenyl)acrylonitrile (3A)**. **M2** (1.80 g, 5 mmol), ethanol (150 mL), p-nitrobenzylcyanide (0.81 g, 5 mmol), and piperidine (0.25 mL) were added to a one-neck flask. The mixture was refluxed at 80 °C for 4 h (monitored by TLC). After cooling to room temperature, the red crystal which had formed was filtered off, washed with ethanol for three times to get 2.00 g red crystal. Yield: 80%. <sup>1</sup>H-NMR (400 MHz, (CD<sub>3</sub>)<sub>2</sub>CO) δ (ppm): 8.32 (d, *J* = 8.80 Hz, 2H), 7.99 (m, 3H), 7.91 (d, *J* = 8.80 Hz, 2H), 7.20 (d, *J* = 9.2 Hz, 4H), 6.98 (d, *J* = 8.80 Hz, 4H), 6.83 (d, *J* = 8.40 Hz, 2H), 4.07 (q, *J* = 7.2 Hz, 4H), 1.38 (t, *J* = 8.80 Hz, 6H). <sup>13</sup>C-NMR (100 MHz, (CD<sub>3</sub>)<sub>2</sub>CO) δ (ppm): 157.88, 152.95, 148.03, 146.17, 142.68, 139.56, 132.55, 129.07, 126.99, 125.05, 124.72, 118.98, 117.58, 116.48, 103.89, 64.30, 15.12. MALDI-TOF Calcd for C<sub>31</sub>H<sub>27</sub>N<sub>3</sub>O<sub>4</sub>, 505.20; Found, 505.28.

**(Z)-3-(4-(bis(4-ethoxyphenyl)amino)phenyl)-2-(4-aminophenyl)acrylonitrile (3B)**. A solution of ethanol (150 mL) with **3A** (1.10 g, 2 mmol) was added to a flask equipped with a magnetic stir, then SnCl<sub>2</sub>·2H<sub>2</sub>O (2.49 g, 11 mmol) was added and the mixture was refluxed for 0.5 h. Neutralized with saturated NaHCO<sub>3</sub> to weak basicity, diluted with water (about 50 mL), and extracted with dichloromethane. The combined organic phase was dried over Na<sub>2</sub>SO<sub>4</sub>, filtered and concentrated to give red oil. Purified by silica gel column chromatography using petroleum (b.p. 60-90 °C)/ethyl acetate (10:1 by volume) to get 0.56 g yellow solid. Yield: 54%. <sup>1</sup>H-NMR (400 MHz, (CD<sub>3</sub>)<sub>2</sub>SO), δ (ppm): 7.69 (d, *J* = 8.80 Hz, 2H), 7.50 (s, 1H), 7.36 (d, *J* = 7.35 Hz, 2H), 7.10 (d, *J* = 8.80 Hz, 4H), 6.94 (d, *J* = 9.20 Hz, 4H), 6.72 (d, *J* = 8.80 Hz, 2H), 6.62 (d, *J* = 8.80 Hz, 2H), 5.51 (s, 2H), 4.01 (q, *J* = 6.80 Hz, 4H), 1.33 (t, *J* = 7.20 Hz, 6H). <sup>13</sup>C-NMR (100 MHz, (CD<sub>3</sub>)<sub>2</sub>SO) δ (ppm): 155.77, 149.57, 145.35, 138.76, 136.68, 129.90, 127.59, 126.23, 125.06, 121.42, 118.94, 117.07,

115.55, 113.93, 106.16, 63.20, 14.64. MALDI-TOF Calcd for  $C_{31}H_{29}N_3O_2$ , 475.23; Found, 475.30.

## Results and discussion

### Structural Studies



**Scheme 1** Synthetic routes of the chromophores **1A-3A** and **1B-3B**

The synthetic routes of the targeted chromophores (**1A-3A** and **1B-3B**) are presented in Scheme 1. The molecule structures are changed from D- $\pi$ -A to D- $\pi$ -D by restoring  $NO_2$  to  $NH_2$ . These six chromophores and their intermediates were prepared *via* the Knoevenagel and Witting-horner reactions in high yield. All the chromophores are soluble in common organic solvents, such as benzene, ethyl acetate, ethanol, acetonitrile, and N,N-dimethylformamide (DMF). They were fully characterized by  $^1H$  and  $^{13}C$ -NMR, mass spectrometry, and elemental analysis. The structures of **1A-3A** and **3B** were also characterized by single crystal X-ray diffraction analysis.

### The crystal structure descriptions of **1A-3A** and **3B**

The crystal structures of the chromophores are shown in Fig. 1-3 and Fig. S1-S3. The crystal data collection and refinement parameters are listed in Table S1. The selected bond distances and angles are given in Table S2. The structure of chromophore **1A** has been reported previously,<sup>39</sup> here is listed for the comparison.

The ORTEP diagram of chromophore **2A** with atom numbering scheme has been depicted in Fig. 1a. As shown in this figure, the central nitrogen (N2) and its three bonded carbon atoms are in distorted pyramidal geometry of the bond angles in the range of 117.2-120.6°. The dihedral angle between the two benzene rings P1 and P2 is 4.37°, which is much smaller than that of **1A** (29.59°), revealing that the

planarity of **2A** is much better than that of **1A** by introducing ethoxy chain to the triphenylamine moiety. Furthermore, the linkage between the rings is quite conjugated with bond lengths of 1.498(6) Å (C23-C22), 1.280(5) Å (C22=C21) and 1.465(5) Å (C21-C20). The bond-length alternation (BLA, the difference between the average lengths of carbon-carbon single and double bonds)<sup>40</sup> across the  $\pi$ -bridge of **2A** is 0.20 Å, which is much smaller than that of **1A** (1.27Å). These structural features suggest that chromophore **2A** possesses a higher delocalization within the molecule and more charge-transfer features of the ground state in the solid state compared with those of **1A**.

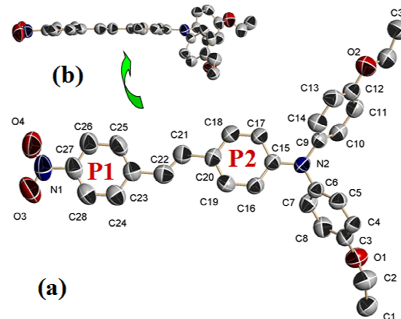


**Fig. 1** (a) ORTEP diagram of **2A**, Hydrogen atoms are omitted for clarity. (b) the side elevation of **2A**

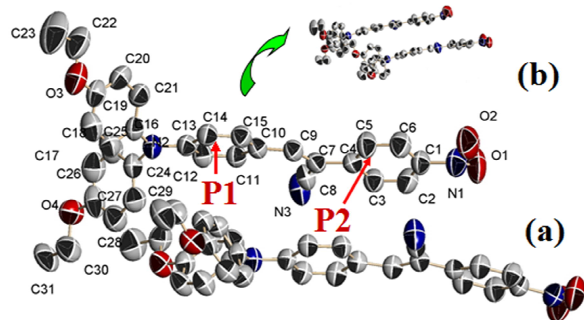


**Fig. 2** (a) ORTEP diagram of **3A**, Hydrogen atoms are omitted for clarity. (b) the side elevation of **3A**

The unit cell of chromophore **3A** contains two molecules as shown in Fig. 2a, while the unit cell of chromophore **3B** contains one molecule (Fig. 3a). Similar to **2A**, around the central nitrogen, three phenyl ring planes are arranged in a pyramidal geometry. The dihedral angles between P1 and P2 (13.58° for **3A** and 12.63° for **3B**) are greater than that of **2A**. Obviously, the cyano group plays an important role in twisting the main structure in comparison with **2A**. However, a direct comparison of the linkage between phenyl rings clearly indicates that the conjugation degree of the chromophore **3A** and **3B** seems to be extended by the cyano group. Noticing that the value of BLA across the  $\pi$ -bridge (0.11 Å for **3A** and 0.12 Å for **3B**) are smaller than that of **2A** (0.20 Å). It is crucial that the BLA has been established as a useful parameter in relation to NLO response.<sup>40</sup>

What's more, cyano group also influences their stack structure. In the case of chromophore **1A** and **2A**, the molecules are fixed into centrosymmetric antiparallel dimers by N-O...H hydrogen bond into a one-dimensional chain

along axis *a* (Fig. S1c and Fig. S2). Differently from them, chromophore **3A** and **3B** are fixed into centrosymmetric antiparallel dimers by weak C-N $\cdots$ H stacking interactions into a one-dimensional chain along axis *b* (Fig. S3 and Fig. 5 3c). Meanwhile, from further inspection of the crystal structure of **3B**, the 2D layer structure is formed through, however, multiple C-H $\cdots$  $\pi$  hydrogen bonds with distance of 2.861 Å between the hydrogen atom in one molecule and the  $\pi$  electron cloud of planar phenyl ring in the other molecule 10 (Fig. 3d). This is a common feature of AIE active molecules.<sup>41, 42</sup> Beside C-H $\cdots$  $\pi$  interaction, there also exists C-H $\cdots$ N, N-H $\cdots$ O hydrogen bonds within the aggregate structure. The various inter-molecular interactions help rigidify the conformation and lock the intramolecular 15 rotations of the phenyl rings. As a result, the excited-state energy consumed by intramolecular rotation is greatly reduced, thus enabling the molecule to emit intensely in the solid state.

Hence, the structural characters of **3B**, such as distorted 20 molecular plane, steric hindrance of cyano segment in case of  $\pi$ - $\pi$  stack, and the smaller value of BLA make the chromophore highly promising candidate for AIE and two-photon absorption materials.

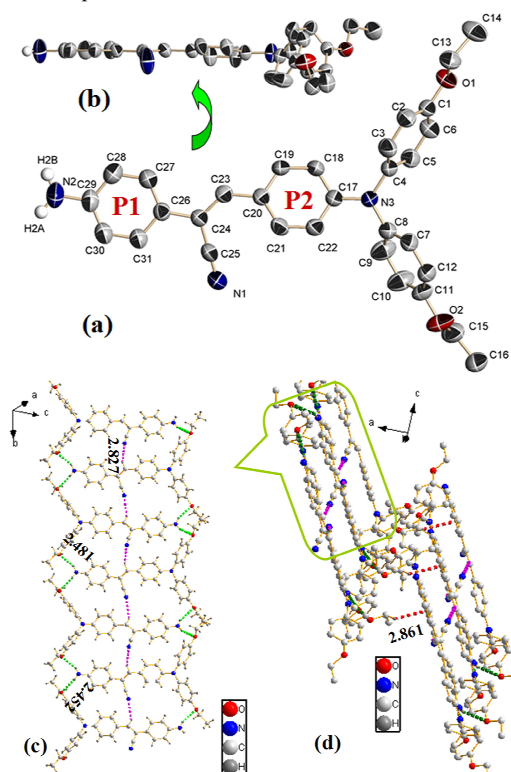


**Fig. 3** (a) ORTEP diagram of **3B**, Hydrogen atoms are omitted for clarity. (b) the side elevation of **3B**. (c) One-dimensional chain of **3B** showing the C-N $\cdots$ H (violet) and C-O $\cdots$ H (blue) along the *b*-axis. (d) Two-dimensional layer structure of **3B** showing the C-H $\cdots$  $\pi$  stacking 25 (red) along the *a*-axis. Hydrogen atoms except H2A, H2B, H13A and H23 are omitted for clarity

### Linear absorption and one-photon excited fluorescence (OPEF).

35 The photophysical data of chromophores **1A-3A** and **1B-3B**

in five different solvents ( $c = 1 \times 10^{-5}$  mol·L<sup>-1</sup>) are collected in Table S3.

**Absorption properties** The absorption spectra of chromophores are shown in Fig. S4. Two major absorption bands can be 40 observed: the band at about 305 nm is attributed to  $\pi$ - $\pi^*$  transition of the triphenylamine moiety, which remains almost unchanged. While the other band locates at about 380-460 nm with stronger intensity, is assigned as intramolecular charge-transfer (ICT) absorption band. This band shows regular red- 45 shift from chromophore **1A(B)** to **3A(B)**, as shown in Fig. 4. This is attributed to the introduction of ethoxyl and cyano groups which increase the electron-donating strength of the end group and extend the conjugation length of the system. Additionally, the introduction of cyano group also leads to the disappearance 50 of short wavelength band of **3A(B)**.

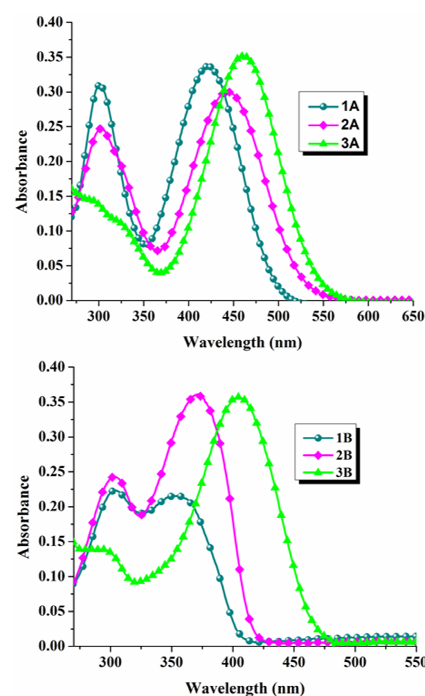


**Fig. 4** Linear absorption spectra of six chromophores ( $1.0 \times 10^{-5}$  mol·L<sup>-1</sup>) in ethyl acetate

**Quantum Chemical Calculations** TD-DFT computational 55 studies were performed to establish the electronic structure of the chromophores and aid in assignment of optical transitions. The energy and composition of ICT are listed in Table 1 and the spatial plots of selected TD-DFT frontier molecular orbitals are shown in Fig. 5 and Fig. S5. the HOMOs (H) of all chromophores are localized on main conjugated framework 60 between the triphenylamine moiety and aniline (or nitrobenzene), and the LUMOs (L) are mainly located on the styrylbenzenamine (or nitro-styrylbenzene) units.

65 As shown in Fig. 5, two transitions of **1B** and **2B** resemble those observed in the experimental linear absorption spectra. The low-energy band originating from H $\rightarrow$ L+1 transition is assigned to intramolecular charge transfer (ICT) transition (aniline $\rightarrow$  triphenylamine moiety), while the high-energy band is assigned

to H→L+2 (**1B**) or H→L+5 (**2B**) transition (ICT) and mixed with the  $\pi$ - $\pi^*$  transition of the triphenylamine. In the case of **3B**, the transition at ca. 396 nm originating from H→L+1 transition is assigned as the ICT transition (triphenylamine→ $\pi$ -bridge).  
 5 Additionally, the energy gap between the H and L of **3B** (0.62 eV) is much smaller than that of **1B** (3.44 eV) and **2B** (3.33 eV), which is caused by the introduction of cyano group in the  $\pi$ -bridge, which may make the electron transfer easily in conjugated systems. This may be the condition for **3B** bearing  
 10 stronger two-photon absorbing active. It is obvious that the optical properties of the chromophores strongly depend on the length of the  $\pi$ -bridge and the nature of peripheral substituting donor groups relying on the theoretical calculation. The results of **1A-3A** are similar to that of **1B-3B** with a satisfying  
 15 agreement with experimental results.

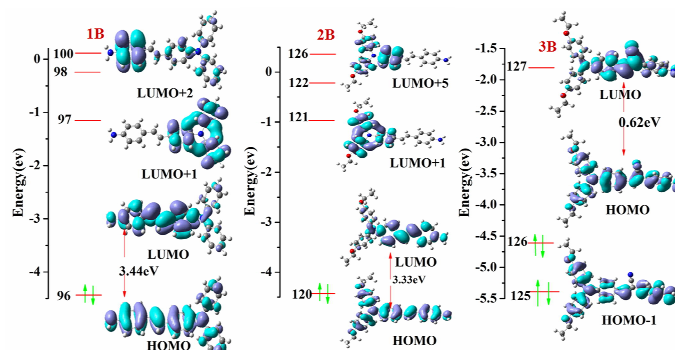


Fig. 5. Molecular orbital energy diagram of **1B-3B**

Table 1 Selected experimental and computed optical data for chromophores **1A-3A** and **1B-3B**

compd	Transitions(S.No.)	OI <sup>a</sup> (Tc) <sup>b</sup>	E (eV) <sup>c</sup>	Cal.λ <sub>max</sub> (nm) <sup>d</sup>	Obs.λ <sub>max</sub> (nm) <sup>e</sup>	f <sup>f</sup>	Character
<b>1A</b>	1	102(H-1)→104(L)	3.2869	377.2	426.3	0.7868	$\pi$ → $\pi^*$ ICT
	2	103(H)→108(L+4)	4.0296	307.7	303.4	0.2042	$\pi$ → $\pi^*$
<b>2A</b>	1	126(H-1)→128(L)	2.7525	450.4	446.7	0.6268	$\pi$ → $\pi^*$ ICT
	2	127(H)→132(L+4)	4.0483	306.3	304.5	0.2063	$\pi$ → $\pi^*$
<b>3A</b>	1	133(H)→135(L+1)	2.6702	464.3	463.6	0.5896	$\pi$ → $\pi^*$ ICT
<b>1B</b>	1	96(H)→100(L+3)	4.1425	299.3	302.1	0.0405	$\pi$ → $\pi^*$
	2	96(H)→98(L+1)	3.6687	337.9	352.4	0.0331	$\pi$ → $\pi^*$ ICT
<b>2B</b>	1	120(H)→122(L+1)	3.4673	357.6	372.2	0.0294	$\pi$ → $\pi^*$ ICT
	2	120(H)→125(L+4)	4.0808	303.8	303.4	0.0428	$\pi$ → $\pi^*$
<b>3B</b>	1	125(H)→127(L+1)	3.1295	396.2	405.5	0.0221	$\pi$ → $\pi^*$ ICT

a: Orbitals involved in the excitations, b: Transition coefficients, c: Excitation energies (eV), d: Calculate peak position of the longest absorption band, e: Observed peak position of the longest absorption band, f: Oscillator Strengths.

## 20 One-photon excited fluorescence (OPEF)

Representative one-photon induced emission spectra of **2B** in different solvents are shown in Fig. 6, the others are included in the supporting information (Fig. S6). These chromophores (especially **1B-3B**) show regular red-shift as the solvent polarity  
 25 increase, indicating that this charge separation increases in the excited state, resulting in a larger dipole moment than that in the ground state, which explains the sensitivity of the emission spectra of these chromophores to solvent polarity.<sup>43</sup> It is noticed that these chromophores exhibit much remarkable bathochromic  
 30 shift in ethanol compared to other solvents, indicating that hydrogen bond interactions may occur between the chromophores and ethanol.

As shown in Fig. 7a, chromophores **1A-3A** and **1B-3B** in benzene all show obvious bathochromic shift from **1A(B)** to  
 35 **3A(B)**, respectively. They are all in agreement with the order of the extension of the  $\pi$ -system: 4-ethoxy-N-(4-ethoxy- phenyl)-N-phenyl aniline > triphenylamine. Meanwhile, noting that **1B-3B** exhibit much stronger fluorescence intensity compared with that of **1A-3A** by changing from nitro into amino. Additionally, it

40 can be seen from Fig. 7b that the fluorescence wavelength of **3B** is evidently red-shift by **2B** and the intensity becomes much weaker, which is due to the introduction of cyano group.

Meanwhile, the time-resolved fluorescence measurements were performed and the detailed data of the fluorescence decay curves  
 45 are listed in Table S3. The experimental errors are estimated to be  $\pm 11\%$  from sample concentrations and instruments. The lifetimes of **1B-3B** in the solution were obtained by monitoring at the monomer emission. The decay behaviors of **1B-3B** were double-exponential manner obtained by monitoring at the  
 50 monomer emission. As shown in Table S3, the weighted mean lifetime of **3B** (0.97 ns) in ethyl acetate is longer than that of **1B** (0.51 ns) and **2B** (0.73 ns). This may be attributed to the larger delocalization, leading to a larger molecular stabilization effect for the excited state.

55 Additionally, the fluorescence lifetime of **3B** in ethyl acetate was calculated by multiplying the corresponding quantum yield on natural lifetime, which could be easily calculated from the known Strickler-Berg equation (eqn. 1).<sup>44</sup> A calculated fluorescence lifetime of 1.02 ns was obtained, which is in

excellent agreement with the experimental value (0.97 ns) and further validate the experimental time-resolved technique.

$$\frac{1}{\tau_0} = 2.88 \times 10^{-9} n^2 \frac{\int I(\tilde{\nu}) d\tilde{\nu}}{\int I(\tilde{\nu}) \tilde{\nu}^{-3} d\tilde{\nu}} \int \frac{\varepsilon(\tilde{\nu})}{\tilde{\nu}} d\tilde{\nu} \quad (1)$$

in which  $n$  is the refractive index,  $I$  is the fluorescence emission,  $\varepsilon$  is the extinction coefficient, and  $\tilde{\nu}$  is the wavenumber. The natural radiative lifetime  $\tau_0$  and the fluorescence lifetime  $\tau$  are related through the quantum yield  $\Phi$  by

$$\Phi = \frac{\tau}{\tau_0} \quad (2)$$

Except for the tunable fluorescence and increased FL lifetime, the exciton-plasmon interaction and energy transfer of **3B** also results in dramatically optimization on NLO activity, such as 2PA and TPEF.

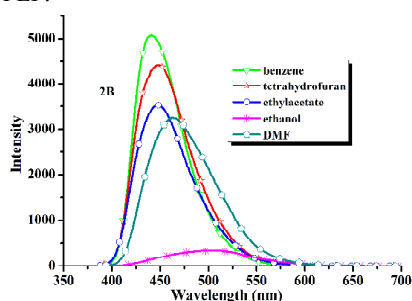


Fig. 6 The one-photon excited fluorescence spectra of **2B** in different solvents

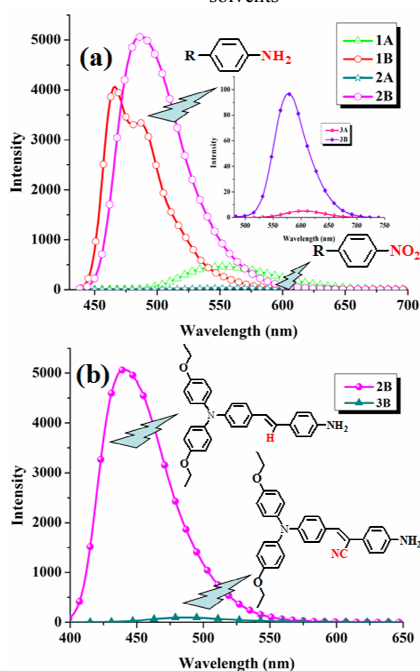


Fig. 7 The one-photon excited fluorescence spectra of **1A-3A**, **1B-3B** (a) and **2B-3B** (b) in benzene

## Aggregation-Induced Enhanced Emission

To investigate the AIE attribute of **3B**, different amounts of water (a poor solvent for **3B**) were added into the pure DMSO solution by defining the water fractions ( $f_w$ ) of 0-99% and then monitored the photoluminescence (PL) change with the excitation wavelength of 503 nm, respectively. Fig. 8a shows

that the emission of **3B** is dramatically weakened with a gradual addition of water into the DMSO and the emission band is bathochromically shifted when  $f_w \leq 50\%$ . The light emission is invigorated from  $f_w \approx 60\%$  and reaches its maximum value at 90% water content, which is 11-fold higher than that in pure DMSO solution. Meanwhile, the emission maximum is gradually red-shifted to 556 nm when  $f_w$  reaches 99%. It is presumable that molecule of **3B** may cluster together to form random, amorphous aggregates in the mixture with low water fractions (0-50%). When the water fraction becomes higher, the chromophore may agglomerate in an ordered fashion to form crystal-like aggregates.<sup>45</sup> This phenomenon is also probably caused by the change of solvent polarity with addition of water at low water fractions, then the water can interact with solute molecules immediately, which would weaken the emission gradually.<sup>46</sup> As can be seen in the inset of Fig. 8a, after reaching a maximum intensity at 90% water content, the PL intensity decreases with increasing water content. This phenomenon was often observed in some compounds with AIE properties, but the reasons remain unclear. There are two possible explanations for this phenomenon: (1) After the aggregation, only the molecules on the surface of the nano-particles emit light and contribute to the fluorescent intensity upon excitation, leading to a decrease in fluorescent intensity. However, the restriction of intramolecular rotation in the aggregation state can enhance light emission. The net outcome of these antagonistic processes depends on which process plays a predominant role in affecting the fluorescent behavior of the aggregated molecules.<sup>47</sup> (2) When water is added, the solute molecules can aggregate into two kinds of nano-particle suspensions: crystal particles and amorphous particles. The former one results in an enhancement in the PL intensity, while the latter leads to a reduction in intensity.<sup>48</sup>

The absorption spectra of **3B** in the DMSO/water mixtures ( $c = 1 \times 10^{-5} \text{ mol}\cdot\text{L}^{-1}$ ) are shown in Fig. 8b. The spectral profiles are significantly changed when  $f_w > 60\%$ , respectively. The intensity of absorption peaks of the compound **3B** positioned at 400 nm gradually decrease with the increasing water content, while the new peak located at about 490 nm emerges afterward, indicating the formation of nanoscopic aggregates of **3B**. The representative scanning electron microscopy (SEM) image in Fig. 9a shows the formation of nano-aggregates of **3B** by the addition of the 90% fraction of water, the image indicates that the AIE dots are well dispersed and have a needle-like with a mean size of about 200 nm. Fig. 9b, c show fluorescence images of **3B** in the DMSO solution, nanoparticle suspension (90% water content) and powder under UV light.

To quantitatively evaluate the AIE effect of **3B**, the quantum efficiency of the solid powder was measured and the value is 7.13%, measured by using an integrating sphere, which are higher than that of **3B** in the solution ( $\Phi < 0.4\%$ ) and manifest its AIE feature.

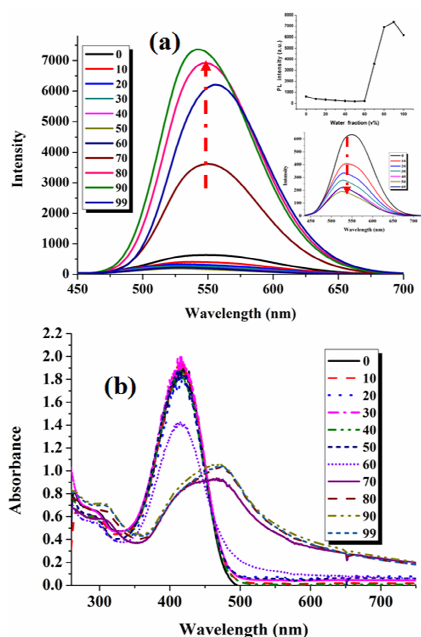


**Fig. 8** PL spectra (a) and Absorption spectra (b) of **3B** in DMSO/water mixtures with different water fraction ( $f_w$ ). The inset depicts the changes of PL peak intensity with different water fractions

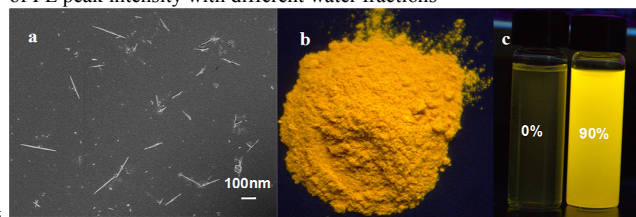


**Fig. 9** (a) SEM image of **3B** in the water/DMSO mixture with 90% water fraction at concentration of  $1 \times 10^{-5}$  M (b) solid powder of **3B** (c) PL emission photos of  $1 \times 10^{-5}$  M in the water/DMSO mixtures with 0% and 90% water concentration under 365 nm UV light illumination.

### Two-photon excited fluorescence (TPEF)

The two-photon excited fluorescence (TPEF) spectra of chromophores **2B** and **3B** were recorded at their maximum excitation wavelength with a pulse duration of 140 fs under 300 mW (milliwatt). The TPEF spectra data of **2B** and **3B** are described in Table S3, which were measured in ethyl acetate ( $c = 1 \times 10^{-3}$  mol·L<sup>-1</sup>).

TPEF spectra of chromophores **2B** and **3B** in ethyl acetate pumped by femtosecond laser pulse at 300 mW at different excitation wavelengths are presented in Fig. S7 (left). Fig. S7 (right) shows logarithmic plots of the fluorescence integral versus pumped power with a slope of 1.93 and 1.97 when the input laser power is increasing, suggesting a two-photon excitation mechanism. As no linear absorption was observed in the range from 680-1080 nm, the emission excited by 700 nm laser wavelength can be attributed to the TPEF mechanism. The TPEF bands located at 500 nm for **2B** and 550 nm for **3B**, which are evidently red-shifted by 52 and 23 nm comparing with those of OPEF in ethyl acetate due to the reabsorption effect. In addition, a red-shift of **3B** compared with **2B** is observed,

revealing that the nature of  $\pi$ -bridge plays an important role in TPEF. It is reasonable that the cyano group substituted on the ethylenic bond increased the electron density of the  $\pi$ -bridge (shown in DFT calculations), favoring the ICT between the core and the two end groups.

The 2PA cross sections ( $\sigma$ ) of chromophores **2B** and **3B** were measured in the wide wavelength range from 680-1050 nm. Fig.10 (left) indicates that in the measured region, the 2PA cross-section  $\sigma$  value of chromophore **3B** is much enhanced compare with **2B**. Furthermore, two-photon action cross-sections ( $\Phi\sigma$ ) are shown in Fig.10 (right), the maximum value are 527 GM for **2B** and 394 GM for **3B**, respectively. Noticing that though the OPEF intensity of **3B** is much lower than that of **2B**, the two-photon action absorption cross section of **3B** is only slightly smaller than that of **2B**. On account of the extended  $\pi$ -system and enhanced intra-molecular charge transfer (ICT) from the triphenylamine to the cyano group. The result proves that the strategy of increasing the ICT effect is an effective approach for enhancing the 2PA cross section of the molecule. Therefore, the value of the 2PA cross section to the functional material can be modulated by simply modify on  $\pi$ -bridge. Significantly, by comparing **3B** with **2B**, it not only shows larger  $\sigma$  and  $\Phi\sigma$  value, but also exhibits higher PL intensity at 90% water content due to AIE property, which spurred us further to explore its potential application in biological imaging.

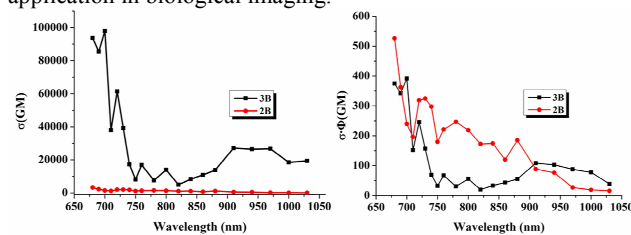


**Fig.10** Two-photon absorption cross section (left) and two-photon action absorption cross section (right) ( $\sigma$ , 1 GM =  $10^{-50}$  cm<sup>4</sup>·s·photon<sup>-1</sup> molecule<sup>-1</sup>) of chromophores **2B** and **3B** in ethyl acetate versus excitation wavelengths of identical energy of 0.30 W

### Two-Photon Microscopy Biological Imaging Application of 3B

Considering the comprehensive merits of the chromophores, we singled out **3B** for biological imaging application research. To analyze the potential of **3B** as an antitumor agent, its cytotoxicity was measured toward the human hepatoma cancer cells (HepG2). The tested chromophore was dissolved in DMSO and then serially diluted in complete culture medium. It is noteworthy that the live cells were stained with **3B**, the cells were active for 24 h during the incubation time (Fig. S8.). The results clearly indicate that HepG2 cells incubated with concentration of 10  $\mu$ M of **3B** remained 90% viable after 24 h of feeding time, demonstrating the superior biocompatibility of **3B**.

To evaluate the internalisation of **3B** in living cells, one- and two-photon fluorescence microscopy micrographs were obtained from HepG2 incubated with **3B**, owing to its relatively lower toxicity toward live cells and two-photon behavior together with AIE property. A bright-field image (Fig. 11a) of each cell was

taken immediately prior to the imaging. To minimize the side effects of organic solvent toward live cells, **3B** was dissolved in DMSO at high concentration and diluted with phosphate buffer solution to a working concentration. OPEF images (Fig. 11b) of each live cell were successfully taken and clearly display the cytoplasm structure. The TPEF images of **3B** (Fig. 11c) exhibit similar cellular cytosol uptake at the excitation wavelength of 700 nm. It shows the remarkable stability of the fluorescence from cellular cytosol as we switch one photon excitation to two-photon excitation. It's worth noting that the TPEF images of **3B** not only exhibit cellular cytosol uptake but also exhibit actin regulatory protein staining. As most of currently commercial available cellular actin probes are membrane impermeable, highly toxic and require pre-fixation, therefore, **3B** might be able to have potential as more safety fluorescence probe for cellular cytosol and actin in two-photon excitation range.<sup>50</sup> Our preliminary confocal microscopy studies reveal that **3B** with function as a luminescent cellular cytosol probe for HepG2 cells being successfully taken up by live cells and clearly emerged from cellular cytoplasm (Fig. 11d, Fig. 11e). We presume that the luminescence from punctuate bright dots outside the nuclei region is because of the aggregation of the complex inside the lysosome. This result demonstrates that the observed lysosome uptake may be due to the presence of the intact **3B**.

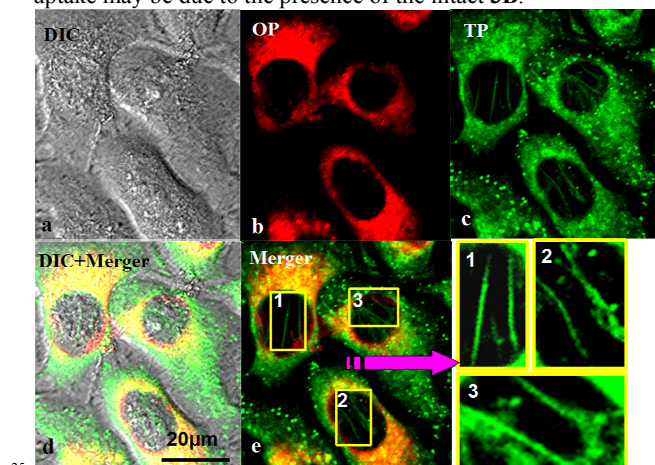


**Fig.11** (a) Bright-field image of HepG2 cells. (b) One-photon image of HepG2 cells incubated with 20 mM **3B** after 30 min of incubation, washed by PBS buffer.  $\lambda_{\text{ex}} = 416$  nm (emission wavelength from 536 to 556 nm). (c) Two-photon image of HepG2 cells incubated with 20 mM **3B** after 30 min of incubation, washed by PBS buffer.  $\lambda_{\text{ex}} = 690$  nm (emission wavelength from 540 nm to 560 nm). (d) The overlay of a-c. (e) The overlay of b-c. Scale bars represent 20  $\mu\text{m}$ .

## Conclusion

A series of triphenylamine derivatives with D- $\pi$ -A (**1A-3A**) or D- $\pi$ -D (**1B-3B**) configuration have been synthesised by convenient method. Their photophysical properties can be tuned by simple modification of electron donor and  $\pi$ -bridge groups, as correlate both experimentally and theoretically. Interestingly, the introduction of cyano-group in chromophore **3B** results in lower OPEF intensity but stronger intensity of TPEF than that of corresponding **2B**. Significantly, **3B** emits intensely upon aggregated formation in water/DMSO mixture, demonstrates a

typical AIE feature. Therefore the simple modification on  $\pi$ -bridge of chromophore **3B** resulting excellent 2PA and AIE properties which pave the way for its biophotonic application. Our initial investigation demonstrates that **3B** is successfully applied to a two-photon fluorescent probe for labeling the cytoplasm and actin regulatory protein in live cells. Finally, it can be said that the research results open a new way to search for applicable new TPA material.

## Acknowledgments

This work was supported by a grant for the National Natural Science Foundation of China (51372003, 21271004, 21275006 and 21271003), the Natural Science Foundation of Anhui Province (1208085MB22, 1308085MB24), Natural Science Foundation of Education Committee of Anhui Province (KJ2012A024), Ministry of Education Funded Projects Focus on returned overseas scholar. The Foundation for Outstanding Youth of the Department of Science and Technology of Anhui Province.

## Notes and references

<sup>a</sup> Department of Chemistry, Key Laboratory of Functional Inorganic Materials Chemistry of Anhui Province, Anhui University, Hefei 230039, P. R. China

E-mail: jywu1957@163.com; yptian@ahu.edu.cn

† Electronic Supplementary Information (ESI) available: CIF files giving X-ray crystallographic data are available free of charge via the Internet at <http://www.ccdc.cam.ac.uk>. CCDC 2A-1006493, 3A-1006514, 3B-1006515.

- P. Chantharasupawong, R. Philip, N. T. Narayanan, P. M. Sudeep, A. Mathkar, P. M. Ajayan, J. Thomas. *J. Phys. Chem. C*, 2012, **116**, 25955-25961
- T. C. Lin, Y. H. Lee, B. R. Huang, C. L. Hu, Y. K. Li. *Tetrahedron*, 2012, **68**, 4935-4949
- C. W. Spangler. *J. Mater. Chem.*, 1999, **9**, 2013-2020
- G. S. He, T. C. Lin, V. K. S. Hsiao, A. N. Cartwright, P. N. Prasad, L. V. Natarajan, V. P. Tondiglia, R. Jakubiak, R. A. Vaia, T. J. Bunning. *Appl. Phys. Lett.*, 2003, **83**, 2733-2735
- W. Dallari, M. S. Abbusco, M. Zanella, S. Marras, L. Manna, A. Diaspro, M. Allione. *J. Phys. Chem. C*, 2012, **116**, 25576-25580
- J. C. Harper, S. M. Brozik, C. J. Brinker, B. Kaehr. *Anal. Chem.*, 2012, **84**, 8985-8989
- L. Yuan, W. Y. Lin, H. Chen, S. S. Zhu, L. W. He. *Angew. Chem. Int. Ed.*, 2013, **52**, 10018-10022
- F. Hammerer, G. Garcia, S. Chen, F. Poyer, S. Achelle, C. F. Debuisschert, M. P. Teulade-Fichou, P. Maillard. *J. Org. Chem.*, 2014, **79**, 1406-1417
- K. Ohta, S. Yamada, K. Kamada. *J. Phys. Chem. A*, 2011, **115**, 105-117
- (a) Y. H. Jiang, Y. C. Wang, J. L. Hua, J. Tang, B. Li, S. X. Qian, H. Tian. *Chem. Commun.* 2010, **46**, 4689-4691; (b) Y. H. Jiang, Y. C. Wang, B. Wang, J. B. Yang, N. N. He, S. X. Qian, J. L. Hua. *Chem. Eur. J.*, 2011, **17**, 2479-2491
- M. Albota, D. Beljonne, J. L. Brédas, J. E. Ehrlich, J. Y. Fu, A. A. Heikal, S. E. Hess, T. Kogej, M. D. Levins, S. R. Marder, D. McCordMaughon, J. W. Perry, H. Röckel, M. Rumi, G. Subramaniam, W. W. Webb, X. L. Wu and C. Xu. *Science*, 1998, **281**, 1653-1657
- G. Bort, T. Gallavardin, D. Ogden, P. Dalko. *Angew. Chem. Int. Ed.*, 2013, **52**, 4526-4537
- Z. Q. Liu, Q. Fang, D. X. Cao, D. Wang. *Org. Lett.*, 2004, **6**, 2933-2936

14. W. Huang, F. S. Tang, B. Li, J. H. Su, H. Tian. *J. Mater. Chem. C*, 2014, **2**, 1141-1148
15. C. D. Entwistle, J. C. Collings, A. Steffen, L.O. Pålsson, A. Beeby, D. Albesa-Jové. *J. Mater. Chem.*, 2009, **19**, 7532-7544
16. P. Ganesan, A. Chandiran, P. Gao, R. Rajalingam, M. Grätzel, M. K. Nazeeruddin. *J. Phys. Chem. C* XXXX, **XXX**, XXX-XXX (dx.doi.org/10.1021/jp5004352)
17. B. A. Reinhardt. *Chem. Mater.*, 1998, **10**, 1863-1874
18. S. W. Thomass, G. D. Joly, T. M. Swager. *Chem. Rev.*, 2009, **109**, 5799-5867
19. (a) S. Kim, Q. D. Zheng, G. S. He, D. J. Bharali, H. E. Pudavar, A. Baev, P. N. Prasad. *Adv. Funct. Mater.*, 2006, **16**, 2317-2323; (b) S. Kim, T. Y. Ohulchanskyy, H. E. Pudavar, R. K. Pandey, P. N. Prasad. *J. Am. Chem. Soc.*, 2007, **129**, 2669-2675
20. R. R. Hu, J. L. Maldonado, M. Rodriguez, C. M. Deng, C. K. M. Jim, J. W. Y. Lam, M. M. F. Yuen, G. R. Ortiz, B. Z. Tang. *J. Mater. Chem.*, 2012, **22**, 232-240
21. Z. Zheng, Z. P. Yu, M. D. Yang, F. Jin, Q. Zhang, H. P. Zhou, J. Y. Wu, Y. P. Tian. *J. Org. Chem.*, 2013, **78**, 3222-3234
22. M. D. Yang, D. L. Xu, W. G. Xi, L. K. Wang, J. Zheng, J. Huang, J. Y. Zhang, H. P. Zhou, J. Y. Wu, Y. P. Tian. *J. Org. Chem.*, 2013, **78**, 10344-10359
23. Z. J. Ning, H. Tian. *Chem. Commun.*, 2009, 5483-5495
24. B. Liu, Q. Zhang, H. J. Ding, J. Y. Wu, Y. P. Tian. *Dyes and Pigments*. 2012, **95**, 149-160
25. Y. H. Jiang, Y. C. Wang, J. L. Hua, J. Tang, B. Li, S. X. Qian, H. Tian. *Chem. Commun.*, 2010, **46**, 4689-4691
26. B. Wang, Y. C. Wang, J. L. Hua, Y. H. Jiang, J. H. Huang, S. X. Qian, H. Tian. *Chem.-Eur. J.*, 2011, **17**, 2647-2655
27. M. Rumi, J. E. Ehrlich, A. A. Heikal, J. W. Perry, S. Barlow, Z. Hu, D. McCord-Maughon, T. C. Parker, H. Rockel, S. Thayumanavan, S. R. Marder, D. Beljonne, J. L. Bredas. *J. Am. Chem. Soc.*, 2000, **122**, 9500-9510
28. S. J. Zheng, L. Beverina, S. Barlow, E. Zojer, J. Fu, L. A. Padilha, C. Fink, O. Kwon, Y. P. Yi, Z. G. Shuai, E. W. V. Stryland, D. J. Hagan, J. L. Bredas, S. R. Marder. *Chem. Commun.*, 2007, 1372-1374
29. (a) W. Huang, F. S. Tang, B. Li, J. H. Su, H. Tian. *J. Mater. Chem. C*, 2014, **2**, 1141-1148; (b) B. K. An, S. K. Kwon, S. D. Jung, S. Y. Park. *J. Am. Chem. Soc.*, 2002, **124**, 14410-14415
30. S. B. Noh, R. H. Kim, W. J. Kim, S. Kim, K. S. Lee, N. S. Cho, H. K. Shim, H. E. Pudavar, P. N. Prasad, *J. Mater. Chem.*, 2010, **20**, 7422-7429
31. J. N. Demas, G. A. Crosby. *Review. J. Phys. Chem.*, 1971, **75**, 991-1024
32. T. G. Gray, C. M. Rudzinski, E. E. Meyer, R. H. Holm, D. G. Nocera. *J. Am. Chem. Soc.*, 2003, **125**, 4755-4770
33. S. K. Lee, W. J. Yang, J. J. Choi, C. H. Kim, S. J. Jeon, B. R. Cho. *Org. Lett.*, 2005, **7**, 323-326
34. C. Xu, W. W. Webb. *J. Opt. Soc. Am. B*, 1996, **13**, 481-491
35. L. Yang, J. K. Feng, A. M. Ren, *J. Org. Chem.*, 2005, **70**, 5987-5996
36. M. J. Frisch, G. W. Trucks, H. B. Schlegel, G. E. Scuseria, M. A. Robb, J. R. Cheeseman, J. A. Montgomery Jr, T. Vreven, K. N. Kudin, J. C. Burant, J. M. Millam, S. S. Iyengar, J. Tomasi, V. Barone, B. Mennucci, M. Cossi, G. Scalmani, N. Rega, G. A. Petersson, H. Nakatsuji, M. Hada, M. Ehara, K. Toyota, R. Fukuda, J. Hasegawa, M. Ishida, T. Nakajima, Y. Honda, O. Kitao, H. Nakai, M. Klene, X. Li, J. E. Knox, H. P. Hratchian, J. B. Cross, C. Adamo, J. Jaramillo, R. Gomperts, R. E. Stratmann, O. Yazyev, A. J. Austin, R. Cammi, C. Pomelli, J. W. Ochterski, P. Y. Ayala, K. Morokuma, G. A. Voth, P. Salvador, J. J. Dannenberg, V. G. Zakrzewski, S. Dapprich, A. D. Daniels, M. C. Strain, O. Farkas, D. K. Malick, A. D. Rabuck, K. Raghavachari, J. B. Foresman, J. V. Ortiz, Q. Cui, A. G. Baboul, S. Clifford, J. Cioslowski, B. B. Stefanov, G. Liu, A. Liashenko, P. Piskorz, I. Komaromi, R. L. Martin, D. J. Fox, T. Keith, M. A. Al-Laham, C. Y. Peng, A. Nanayakkara, M. Challacombe, P. M. W. Gill, B. Johnson, W. Chen, M. W. Wong, C. Gonzalez, J. A. Pople, Gaussian 03, Revision B.04, Gaussian, Inc., Pittsburgh, PA, 2003
37. G. M. Sheldrick, SHELXL97, Program for Crystal Structure Refinement, University of Göttingen, Göttingen, Germany, 1997
38. H. P. Zhou, Z. Zheng, G. Y. Xu, Z. P. Yu, X. F. Yang, L. H. Cheng, X. H. Tian, L. Kong, J. Y. Wu, Y. P. Tian. *Dyes and Pigments.*, 2012, **90**, 570-582
39. Z. W. Zhang, Y. Q. Liu, Y. C. Zhu, J. Y. Wu. *Acta Cryst.*, 2011, **E68**, o1933
40. S. R. Marder. *Chem. Commun.*, 2006, 131-134
41. Z. Zheng, Z. P. Yu, M. D. Yang, F. Jin, Q. Zhang, H. P. Zhou, J. Y. Wu, Y. P. Tian. *J. Org. Chem.*, 2013, **78**, 3222-3234
42. X. Y. Shen, W. Z. Yuan, Y. Liu, Q. L. Zhao, P. Lu, Y. G. Ma, I. D. Williams, A. J. Qin, J. Z. Sun, B. Z. Tang. *J. Phys. Chem. C*, 2012, **116**, 10541-10547
43. H. P. Zhou, F. X. Zhou, P. Wu, Z. Zheng, Z. P. Yu, Y. X. Chen, Y. L. Tu, L. Kong, J. Y. Wu, Y. P. Tian. *Dyes and Pigments*. 2011, **91**, 237-247
44. (a) K. D. Belfield, M. V. Bondar, A. R. Morales, X. Yue, G. Luchita, O. V. Przhonska. *J. Phys. Chem. C*, 2012, **116**, 11261-11271; (b) S. J. Strickler, R. A. Berg. *J. Chem. Phys.* 1962, **37**, 814-822.
45. H. Tong, Y. Hong, Y. Dong, Y. Ren, M. Haeussler, J. W. Y. Lam, K. S. Wong, B. Z. Tang. *J. Phys. Chem. B*, 2007, **111**, 2000-2007
46. X. Q. Zhang, Z. G. Chi, X. Zhou, S. W. Liu, Y. Zhang, J. R. Xu. *J. Phys. Chem. C.*, 2012, **116**, 23629-23638
47. S. Dong, Z. Li, J. Qin. *J. Phys. Chem. B.*, 2009, **113**, 434-441
48. Z. Y. Yang, Z. G. Chi, T. Yu, X. Q. Zhang, M. N. Chen, B. J. Xu, S. W. Liu, Y. Zhang, J. R. Xu. *J. Mater. Chem.*, 2009, **19**, 5541-5546
49. D. Ding, C. C. Goh, G. X. Feng, Z. J. Zhao, J. Liu, R. R. Liu, N. Tomczak, J. L. Geng, B. Z. Tang, L. G. Ng, B. Liu. *Adv. Mater.*, 2013, **25**, 6083-6088
50. Z. Q. Ji, Y. J. Li, T. M. Pritchett, N. S. Makarov, J. E. Haley, Z. J. Li, M. Drobizhev, A. Rebane, W. F. Sun. *Chem. Eur. J.*, 2011, **17**, 2479-2491

## Graphical abstract

One- and two-photon fluorescence properties of six chromophores were successfully tuned by different electron donors and  $\pi$ -bridges, the simple structure modify of **3B** resulting in a significant AIE effect and large 2PA action cross section, being promising in bioimaging applications

